Inorganic Chemistry

Article

pubs.acs.org/IC

New Structural Types of Mn_{16} Single-Molecule Magnets: W-Shaped Topology from Reductive Aggregation

Annaliese E. Thuijs, Philippa King, Khalil A. Abboud, and George Christou*

Department of Chemistry, University of Florida, Gainesville, Florida 32611-7200, United States

Supporting Information

ABSTRACT: Two new Mn_{16} clusters are reported: $[Mn_{16}O_{10}(OH)_3(OMe)_8(O_2CPhBu^t)_{17}(MeOH)_5]$ (**2**) and $[Mn_{16}O_{16}(OMe)_6(O_2CPh)_{12}(NO_3)_4(MeOH)_2(H_2O)_4]$ (**3**). The complexes were obtained by reductive aggregation of MnO_4^- in CH_2Cl_2/MeOH, and oxidation of Mn^{II} and preformed $(N^nBu_4)[Mn_4^{III}O_2(O_2CPh)_9(H_2O)]$ with Ce^{IV}, respectively. The core of **2** has a Mn_{16}^{III} core with an unusual 1:2:3:4:3:2:1 layer structure and a W-shaped pleated topology, whereas **3** contains a central 2 × 3 Mn_6^{IV} planar grid held within a nonplanar Mn_{10}^{III} loop and is a rare example of a complex with nitrate ions bridging like carboxylate ions. Variable-temperature, solid-state dc susceptibility, and ac susceptibility studies reveal that **2** and **3** possess $S = 12$ and $S = 8$ ground states, respectively. Fits of dc magnetization data collected over a temperature range of 1.8−4.0 K and a magnetization range of 0.1−4 T were fit to give $S = 12$, $D = -0.16(2)$ cm^{-1}, $g = 1.98(3)$ for **2** and $S = 8$, $D = -0.22(1)$ cm^{-1}, $g = 1.99(2)$ for **3**, where D is the axial zero-field splitting parameter. The ac in-phase ($\chi_M'T$) susceptibility below 15 K confirmed the ground-state spin values of **2** and **3**, as determined from dc data, and the appearance of frequency-dependent out-of-phase (χ_M'') signals revealed that both complexes are new single-molecule magnets (SMMs). Fits of the ac data gave $U_{eff} = 49.7(1)$ K and $\tau_0 = 4.32 \times 10^{-9}$ s for **2** and $U_{eff} \approx 14.0 \pm 2$ cm^{-1} and $\tau_0 \approx 3.2 \pm 0.5 \times 10^{-8}$ s for **3**, where U_{eff} is the effective barrier to magnetization relaxation and τ_0 is the pre-exponential factor. Thus, complexes **2** and **3** are two new members of a growing family of Mn_{16} clusters, and two new examples of high-nuclearity SMMs, with the U_{eff} for **2** approaching the value for the prototypical SMM family, $[Mn_{12}O_{12}(O_2CR)_{16}(H_2O)_4]$.

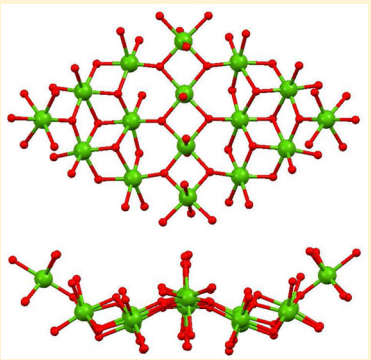

INTRODUCTION

The field of single-molecule magnets (SMMs) continues to attract great interest from many groups.[1,2] It represents an alternative, bottom-up approach to nanoscale magnetism and brings all the advantages of molecular chemistry to this important area of molecular nanoscience, such as monodispersity, solubility, and a shell or organic ligands that can readily be modified using standard solution chemistry methods. Of particular importance and utility is the crystallinity of molecular compounds that provides high-precision structural data via single-crystal X-ray crystallography and highly ordered assemblies for detailed study in the solid state by a variety of chemical and physical methods. The field has expanded greatly in the last two decades from its beginnings in polynuclear Mn and Fe oxo cluster chemistry, through various mixed-metal combinations, to the recent activity in homometallic lanthanide[3] and actinide chemistry,[4,5] as well as mononuclear 3d SMMs,[6] which among other things have led to a dinuclear SMM with the currently highest magnetization hysteresis blocking temperature (T_B) of 14 K in the radical-bridged complex $[Tb_2(N_2)\{N(SiMe_3)_2\}_4(thf)_2]^-$.[7]

A crucial benefit of crystalline SMMs, which represent ordered assemblies of monodisperse magnetic particles, has been the impact on the quantum physics of nanomagnetism. Several novel phenomena have been discovered from ultralow-temperature studies on single crystals of SMMs, such as quantum tunneling of the magnetization vector (QTM),[8] exchange-biased QTM,[9] quantum superposition states and entanglement,[10] quantum phase interference,[11] and others. Most of these would have been extremely difficult, if not impossible, to identify using traditional magnetic nanoparticles, and their experimental discovery was thus directly related to the molecular advantages of SMMs, especially the modification of the ligand shell to allow optimization of a molecular crystal for a particular study, with respect to parallel alignment of all molecules, intermolecular separations, local site-symmetry, etc.

The interest in SMMs has also stimulated much new synthetic methodology development as chemists have sought ways to access new types of SMMs with improved properties.[12] As a consequence, many molecules have been discovered that are very interesting structurally or magnetically, even if they are not SMMs or only poor ones. These include many higher nuclearity clusters with remarkably large ground state spin S values, the majority in Mn chemistry.[13] Examples include Mn_{17},[14] Mn_{19},[15] and Mn_{25},[16] which have S values ranging from $S = {}^{51}/_2$ up to $S = {}^{83}/_2$, although only small D values are observed because of the inverse relationship between S and D.[17] Also note that the structural aesthetics of polynuclear SMM clusters and related species are another facet that has a

Received: July 13, 2015
Published: September 9, 2015

DOI: 10.1021/acs.inorgchem.5b01553
Inorg. Chem. 2015, 54, 9127−9137

tendency to not be emphasized but, nevertheless, is an important chemical aspect of the field, from the beautiful snowflake-like structure of $[Mn_{12}O_{12}(O_2CMe)_{16}(H_2O)_4]$ (**1**),[18] which is the first (and still most well-studied) SMM, to that of the giant Mn_{84} torus,[19] and aggregates of magnetic units such as wheels.[20,21]

For all the above-mentioned reasons, we continue to concentrate some of our efforts in seeking new polynuclear magnetic molecules with interesting structures and/or properties, and we still find Mn cluster chemistry to be a rich source of such materials. Among the several prior synthetic methods employed for the synthesis of homometallic manganese SMMs have been (i) comproportionation of Mn^{II} and Mn^{VII}, usually a Mn^{2+} source and MnO_4^- in some suitably chosen ratio,[22] and (ii) reductive aggregation of MnO_4^- in the presence of MeOH.[23] Both procedures have been fruitful and, indeed, are related in the sense that the first uses Mn^{2+} to reduce Mn^{VII}, whereas the second uses MeOH. This latter method led to a new type of Mn_{12} SMM complex, $(NBu^n_4)_2[Mn_{12}O_{12}(OMe)_2(O_2CPh)_{16}(H_2O)_2]$,[24] and since then, two other MeO^--containing Mn_x clusters,[25,26] which have also been new SMMs. A subsequent procedure replacing the Mn^{VII} with Ce^{IV} in method (i) led to the first Ce/Mn clusters some years ago[27] and initiated what has now become a large field of Ce/Mn cluster chemistry.[28−31] The present work has involved both an extension of our previous interest in reductive aggregation and a new approach involving the oxidation of a preformed Mn^{III}_4 compound with Ce^{IV}.

Herein, we report the syntheses, structures, and magnetic properties of two new high nuclearity Mn_{16}clusters. One has an unprecedented and fascinating pleated structure and has been found to be a SMM with a blocking temperature almost as large as that of **1**. The other is a rare example of a Mn cluster with mixed carboxylate and nitrate ligation, and it is also an SMM.

EXPERIMENTAL SECTION

Synthesis. All manipulations were performed under aerobic conditions using chemicals as received (4-^{t}Bu-benzoic acid (99%) from Aldrich; $Mn(NO_3)_2{\cdot}4H_2O$ and $(NH_4)_2[Ce(NO_3)_6]$ (99%) from ACROS). $N^nBu_4MnO_4$[32] and $(N^nBu_4)[Mn_4O_2(O_2CPh)_9(H_2O)]$[33] were prepared as described elsewhere.

*$[Mn_{16}O_{10}(OH)_3(OMe)_8(O_2CPhBu^t)_{17}(MeOH)_5]$ (**2**).* To a warm solution of 4-^{t}Bu-benzoic acid (3.74 g, 21 mmol) in CH_2Cl_2/MeOH (3:1 v/v, 20 mL) was slowly added $N^nBu_4MnO_4$ (0.50 g, 1.4 mmol) in small portions. The resulting solution was stirred for 2 h during which time it changed from purple to dark brown. The solution was cooled, filtered, and the filtrate left undisturbed for 5 days during which time black-brown needles of **2**·*x*MeOH·*x*CH_2Cl_2 formed. The crystals were maintained in the mother liquor for X-ray crystallographic analysis, and collected by filtration, washed with toluene, and dried under vacuum for other solid-state studies. The yield was 40%−45% (0.24−0.27 g) based on Mn. Anal. Calc. for **2**·MeOH ($C_{201}H_{272}Mn_{16}O_{61}$) (%): C, 53.14; H, 6.03; N, 0.00. Found: C, 53.12; H, 6.01; N, 0.03. Selected IR data (KBr, cm^{-1}): 3422(mb), 2362(m), 2336(m), 1635(w), 1523(mb), 1384(vs), 1022(w), 668(s), 612(mb), 532(m).

*$[Mn_{16}O_{16}(OMe)_6(O_2CPh)_{12}(NO_3)_4(MeOH)_2(H_2O)_4]$ (**3**).* To a stirred dark brown solution of $(N^nBu_4)[Mn_4O_2(O_2CPh)_9(H_2O)]$ (1.0 g, 0.62 mmol) and $Mn(NO_3)_2{\cdot}4H_2O$ (0.040 g, 0.16 mmol) in $MeNO_2$/MeOH (25:1 v/v, 26 mL) was slowly added solid $(NH_4)_2[Ce(NO_3)_6]$ (0.26 g, 0.47 mmol). The resulting solution was stirred for an additional 6 h and filtered, and the filtrate was left undisturbed for eight days, during which time black single needlelike crystals of **3**·4$MeNO_2$ formed. The crystals were kept in the mother liquor for X-ray crystallographic analysis, and collected by filtration, washed with hexanes, and dried under vacuum for other solid-state studies. The yield was 35% (0.15 g) based on Mn. Anal. Calc. for **3**·2$MeNO_2$ ($C_{94}H_{100}Mn_{16}N_6O_{68}$) (%): C, 34.23; H, 3.13; N, 2.61. Found: C, 34.41; H, 3.07; N, 2.56. Selected IR data (KBr, cm^{-1}): 1762(b), 1688(b), 1599(m), 1384(b), 1178(s), 1071(m), 1042(s), 1026(s), 934(b), 825(s), 817(s), 741(b), 709(m), 682(b), 598(b), 518(b).

X-ray Crystallography. Data on **2**·*x*MeOH·*x*CH_2Cl_2 were collected at 173 K on a Siemens SMART PLATFORM equipped with a CCD area detector and a graphite monochromator utilizing Mo Kα radiation (λ = 0.71073 Å). Data on **3**·4$MeNO_2$ were collected at 100 K on a Bruker DUO diffractometer, using Mo Kα radiation and an APEXII CCD area detector. Suitable crystals were attached to glass fibers using silicone grease and transferred to a goniostat, where they were cooled to the indicated temperatures. The structures were solved by direct methods in SHELXTL6 and refined on F^2 using full-matrix least-squares cycles. For **2**·*x*MeOH·*x*CH_2Cl_2, cell parameters were refined using 8192 reflections. A full sphere of data (1850 frames) was collected using the ω-scan method (0.3° frame width). The first 50 frames were remeasured at the end of data collection to monitor instrument and crystal stability (maximum correction on *I* was <1%). Absorption corrections by integration were applied based on measured indexed crystal faces. For **3**·4$MeNO_2$, raw data frames were read by SAINT[34] and integrated using 3D profiling algorithms. The resulting data were reduced to produce *hkl* reflections and their intensities and estimated standard deviations. The data were corrected for Lorentz and polarization effects, and numerical absorption corrections were applied based on indexed and measured faces. Crystal data and structure refinement parameters are listed in Table 1.

Table 1. Crystal Data and Structure Refinement Parameters for 2 and 3

	2·20MeOH·20CH_2Cl_2	**3**·4$MeNO_2$
formula[a]	$C_{240}H_{384}Cl_{40}Mn_{16}O_{80}$	$C_{96}H_{102}Mn_{16}N_8O_{72}$
fw, g mol^{-1}	6846.51	3398.90
space group	$P\bar{1}$	$P\bar{1}$
a, Å	19.9744(2)	13.100(3)
b, Å	24.981(2)	14.423(3)
c, Å	30.850(3)	19.361(4)
α, deg	103.733(2)	105.132(5)
β, deg	104.435(2)	107.098(4)
γ, deg	104.396(2)	100.648(5)
V, Å^3	12684(2)	3236.7(1)
Z	2	1
T, K	173(2)	100(2)
radiation, Å[b]	0.71073	0.71073
ρ_{calc}, g cm^{-3}	1.662	1.744
μ, mm^{-1}	1.184	1.606
*R*1[c,d]	0.0961	0.0581
*wR*2[e]	0.2258	0.1160

[a]Including solvent molecules. [b]Graphite monochromator. [c]$I > 2\sigma(I)$. [d]$R1 = 100\sum(||F_o| - |F_c||)/\sum|F_o|$. [e]$wR2 = 100[\sum[w(F_o^2 - F_c^2)^2]/\sum[w(F_o^2)^2]]^{1/2}$, $w = 1/[\sum^2(F_o^2) + [(ap)^2 + bp]$, where $p = [\max(F_o^2, O) + 2F_c^2]/3$.

For **2**·*x*MeOH·*x*CH_2Cl_2, the asymmetric unit consists of the Mn_{16} cluster and a best estimate of 20 MeOH and 20 CH_2Cl_2 solvent molecules. The latter were severely disordered and could not be modeled properly, thus program SQUEEZE,[35] which is part of the PLATON[36] package of crystallographic software, was used to calculate the solvent disorder area and remove its contribution to the overall intensity data. The H atoms on the coordinated MeOH and H_2O/OH^-(O1) were not located and not included in the final refinement cycle, which refined 1606 parameters using 46 727 reflections with $I > 2\sigma(I)$ to yield R_1 and wR_2 of 9.08% and 21.29%, respectively. The non-hydrogen atoms were treated anisotropically, whereas H atoms were placed in calculated, ideal positions and refined as riding on their respective C atoms.

DOI: 10.1021/acs.inorgchem.5b01553
Inorg. Chem. 2015, 54, 9127−9137

For **3**·4MeNO$_2$, the asymmetric unit consists of a half Mn_{16} cluster and two $MeNO_2$ solvent molecules. The latter were disordered and could not be modeled properly; thus, the program SQUEEZE was again used. H atoms on O20 and O30 were obtained from a difference Fourier map and refined as riding on their respective O atoms. H atoms on the disordered water ligand O29 could not be located and were not included in the final refinement cycles. There are three regions of disorder in the cluster: the Me on O25 was refined in two parts, as were groups of atoms C41−C47 and C22−C27. In the final cycle of refinement, 735 parameters were refined using 11 859 reflections (4664 with $I > 2\sigma(I)$) to yield R_1 and wR_2 values of 5.81% and 11.60%, respectively.

Other Studies. Infrared spectra were recorded in the solid state (KBr pellets) on a Nicolet Nexus 670 FTIR spectrometer in the 400−4000 cm^{-1} range. Elemental analyses (C, H, and N) were performed by the in-house facilities of the University of Florida Chemistry Department. Variable-temperature dc and ac magnetic susceptibility data were collected on vacuum-dried solids using a Quantum Design MPMS-XL SQUID susceptometer equipped with a 7 T magnet and operating in the 1.8−300 K range. Samples were embedded in solid eicosane in a gel capsule to prevent torqueing. Pascal's constants[37] were used to estimate the diamagnetic corrections, and contributions from the eicosane and gel capsule were measured as a blank; these were subtracted from the experimental susceptibility to give the molar paramagnetic susceptibility (χ_M). Magnetization versus field and temperature data were fit using the MAGNET program.[38]

RESULTS AND DISCUSSION

Syntheses. Syntheses utilizing the reductive aggregation of MnO_4^- are carried out in the presence of MeOH and a large excess of carboxylic acid. The former acts as the reducing agent and a potential source of MeO^- ligands, and the latter helps prevent the formation of manganese oxides and/or hydroxides, as well as providing carboxylate ligands. In the present work, dissolution of $N^nBu_4MnO_4$ in a MeOH/CH_2Cl_2 (1:3 v/v) solution of 4-^{t}Bu-benzoic acid gave a dark brown solution, from which was subsequently isolated $[Mn_{16}O_{10}(OH)_3(OMe)_8(O_2CPh^tBu)_{17}(MeOH)_5]$ (**2**; $16Mn^{III}$) in 40%−45% yield. CH_2Cl_2 was added to increase the solubility of the acid. The reaction is clearly a very complicated one, but the main features are summarized in eq 1 and involve reduction of MnO_4^- by

$$16MnO_4^- + 64e^- + 86RCO_2H + 13MeOH \rightarrow 69RCO_2^- + 40H_2O + 11OH^- + [Mn_{16}O_{10}(OH)_3(OMe)_8(O_2CPh^tBu)_{17}(MeOH)_5] \quad (1)$$

solvent molecules, triggering aggregation by oxide-bridge formation. Except for the identity of the carboxylate and the solvent mixture, the procedure is similar to that used previously,[26] which also gave some Mn_{16} clusters, but of a very different structural type than **2**.

We have recently also been exploring an extension of our previous work, using Ce^{IV} instead of Mn^{VII} as the oxidizing agent. These are again complicated cluster aggregation reactions that have led to a variety of Ce/Mn clusters but also homometallic Mn ones, e.g., the recent synthesis of $[Mn_{12}O_{12}(O_2CMe)_{12}(NO_3)_4(H_2O)_4]$, a new member of the Mn_{12} family of SMMs, by the oxidation of Mn^{II} acetate by Ce^{IV} in the presence of an excess of acetic acid.[39] In the present work, we have employed, for the first time, the preformed Mn^{III} cluster $(N^nBu_4)[Mn_4O_2(O_2CPh)_9(H_2O)]$, as well as Mn^{II} nitrate in a reaction with $(NH_4)_2[Ce(NO_3)_6]$[40] in an approximately 4:1:3 ratio in $MeNO_2$/MeOH (25/1 v/v). This gave a dark brown solution, from which $[Mn_{16}O_{16}(OMe)_6(O_2CPh)_{12}(NO_3)_4(MeOH)_2(H_2O)_4]$ (**3** was obtained; $Mn_6^{IV}Mn_{10}^{III}$) in 35% yield. This reaction ratio was the one that was found to give the cleanest product in highest yield, even though it generates a $Mn^{3.11+}$ average (eq 2), which is lower than the $Mn^{3.38+}$ in **3**.

$$4Mn_4^{3+} + Mn^{2+} + 3Ce^{4+} \rightarrow 17Mn^{3.11+} + 3Ce^{III} \quad (2)$$

After structural identification of **3**, we investigated whether it might be possible to replace the MeO^- ligands with OH^- via the addition of tiny amounts of water to **3** dissolved in MeCN, but the only isolable product was well-known $[Mn_{12}O_{12}(O_2CPh)_{16}(H_2O)_4]$ in low (<10%) yield.

Description of Structures. The structure and a stereopair of **2** are shown in Figure 1, and two views of its core are shown in Figure 2. Selected distances and angles are listed in Table 2 and Table S1 in the Supporting Information.[41] The core is composed of 16 Mn^{III} atoms bridged by 10 μ_3-O^{2-}, 8 μ-MeO^-, and 2 μ-OH^- groups. The Mn atoms are arranged in rows with a 1:2:3:4:3:2:1 pattern, and the overall core structure is pleated to give an unusual W-shape. Alternatively, the core can be described as arising from edge-fused Mn_3 triangular units. The Mn oxidation states and O protonation levels were determined from charge considerations and bond valence sum (BVS) calculations (see Table 3). In addition, all Mn atoms exhibit clear Jahn−Teller (JT) elongations (bold bonds in Figure 2b). Peripheral ligation about the core consists of 16 μ- and one μ_3-carboxylate groups, four terminal MeOH groups, and two final terminal groups at the two ends of the molecule that we assign as another MeOH (O57) on Mn16 and an OH^- (O1) on Mn1. The BVS values for O57 and O1 of 1.06 and 1.22, respectively, are as expected for monoprotonated groups. Both the MeOH

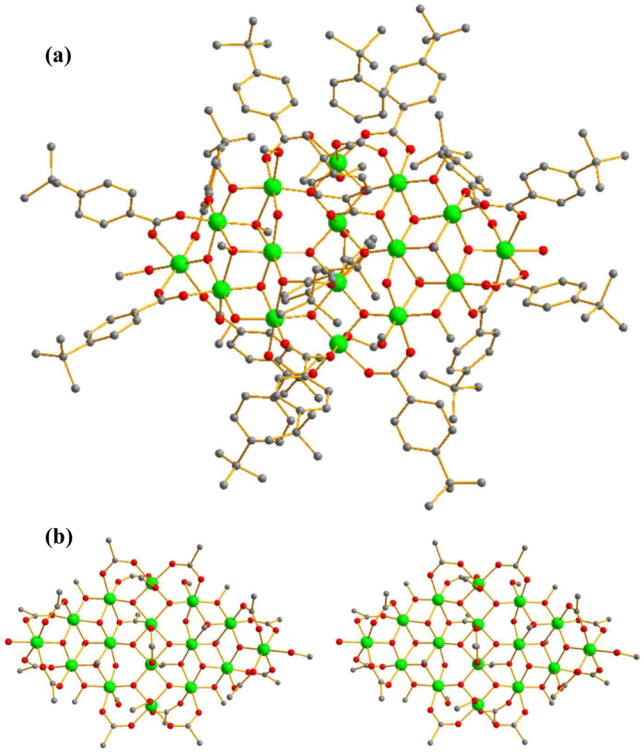

Figure 1. Schematics of (a) the complete structure of complex **2** and (b) a stereopair, with only the *ipso* C atom of each phenyl ring shown (for the sake of clarity). Color code: Mn^{III}, green; O, red; C, gray. H atoms have been omitted for the sake of clarity.

DOI: 10.1021/acs.inorgchem.5b01553
Inorg. Chem. 2015, 54, 9127−9137

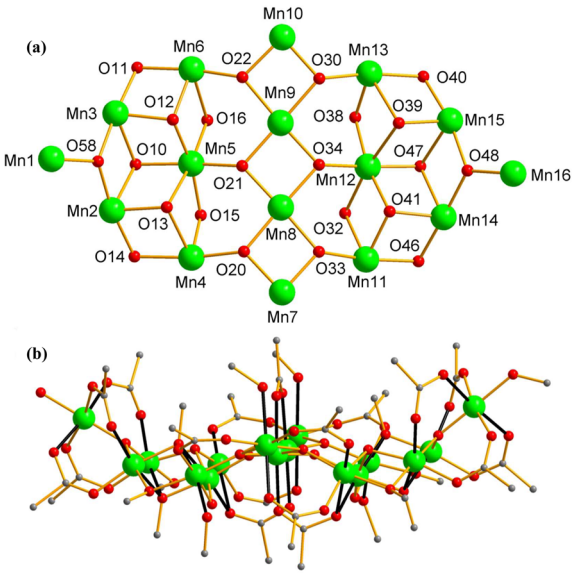

Figure 2. Schematics of (a) the labeled core of **2** viewed along the virtual C_2 axis, and (b) a side view emphasizing the W-shape and the location of the Mn^{III} JT elongation axes (thicker, black bonds). Color code: Mn^{III}, green; O, red; C, gray. H atoms have been omitted for the sake of clarity.

and OH^- groups are involved in intermolecular OH···O hydrogen bonding with carboxylate O atoms on neighboring molecules (O57···O53 = 2.617(16) Å, O1···O4 = 2.787(16) Å). In addition, there are four intramolecular hydrogen bonds in the molecule: two involve bridging OH^- (O15–H···O31 = 2.614(16) Å; O38–H···O28 = 2.573(16) Å) and two involve terminal MeOH groups (O17–H···O43 = 2.654(16) Å; O37–H···O26 = 2.719(16) Å) hydrogen bonding with carboxylate O atoms. The BVS of these OH^- and MeOH O atoms are all below ~1.2, as expected for a monoprotonated O atom. Finally, the cluster has virtual C_2 symmetry, if the difference in terminal ligands on Mn1 and Mn16 is ignored, and we note that the hydrogen bonding involving these terminal ligands and carboxylates of the neighboring molcules forms a zigzag chain (Figure S1 in the Supporting Information).

The Mn^{3+} JT elongation axes are not oriented randomly. Instead, many are parallel or at an acute angle to the virtual C_2 (z) axis of the molecule, i.e., none are perpendicular to this axis. The JT axes of the four central Mn7–Mn10 atoms are aligned essentially parallel to the C_2 axis, and the remaining twelve Mn atoms are aligned between 44.5° (Mn16) and 53.7° (Mn1) to the mean vertical plane containing the central Mn7–Mn10. Thus, it is anticipated that (i) the virtual C_2 axis should be the magnetic easy axis and (ii) the molecule should possess significant magnetoanisotropy, as reflected in the magnitude of the zero-field splitting (zfs) parameter, D (vide infra).

The structure of **3** as a stereopair and two views of its core are shown in Figure 3, and selected distances and angles are listed in Table 4, as well as Table S2 in the Supporting Information. The $[Mn_{16}O_{16}(OMe)_6]^{16+}$ core contains a central planar gridlike Mn^{IV}_6 unit bridged by two μ-O^{2-}, four μ_3-O^{2-} and four μ_2-OMe^- groups above and below the Mn_6 plane. This central $[Mn^{IV}_6O_6(OMe)_4]^{16+}$ unit is held within a nonplanar loop of 10 Mn^{III} atoms by 10 μ_3-O^{2-} ions; two of these, Mn3 and Mn3′, become coplanar with the central Mn_6. With regard to **2**, the Mn oxidation states and O protonation levels were determined by charge considerations, Mn^{III} JT elongation axes, and BVS calculations (Table 3). The peripheral ligation is completed by 12 η^1:η^1:μ-benzoates, four η^1:η^1:μ-nitrates, four terminal H_2O, and two terminal MeOH groups. The complete cluster has C_i symmetry.

Table 2. Selected[a,b] Core Interatomic Distances for Complex 2

atom pairing	interatomic distance (Å)	atom pairing	interatomic distance (Å)
Mn1···Mn2	3.221(4)	Mn11···Mn12	3.101(3)
Mn2···Mn3	3.225(4)	Mn11···Mn14	2.930(4)
Mn2···Mn4	3.099(4)	Mn12···Mn13	3.108(4)
Mn2···Mn5	3.175(4)	Mn12···Mn14	3.061(4)
Mn3···Mn5	3.098(4)	Mn12···Mn15	3.180(4)
Mn3···Mn6	2.947(4)	Mn13···Mn15	3.117(4)
Mn4···Mn5	3.146(4)	Mn14···Mn15	3.212(4)
Mn7···Mn8	2.875(4)	Mn8–O33	1.948(10)
Mn8···Mn9	2.811(3)	Mn9–O34	1.893(10)
Mn9···Mn10	2.865(3)	Mn9–O21	1.914(10)
Mn1–O58	1.893(10)	Mn9–O30	1.957(9)
Mn2–O58	1.850(11)	Mn9–O22	1.988(10)
Mn2–O13	1.938(10)	Mn10–O30	1.860(10)
Mn2–O14	1.954(12)	Mn10–O22	1.877(10)
Mn2–O10	2.264(12)	Mn11–O33	1.871(11)
Mn3–O58	1.935(9)	Mn11–O41	1.904(10)
Mn3–O12	1.945(10)	Mn11–O46	1.909(11)
Mn3–O11	1.958(10)	Mn11–O42	2.007(12)
Mn3–O10	2.243(11)	Mn12–O34	1.870(11)
Mn4–O20	1.869(10)	Mn12–O47	1.902(11)
Mn4–O15	1.926(10)	Mn12–O38	1.951(9)
Mn4–O14	1.952(11)	Mn12–O41	1.970(9)
Mn4–O13	2.180(10)	Mn12–O32	2.217(10)
Mn5–O21	1.857(11)	Mn12–O39	2.260(10)
Mn5–O12	1.920(11)	Mn13–O30	1.873(10)
Mn5–O10	1.943(10)	Mn13–O40	1.896(12)
Mn5–O15	1.946(11)	Mn13–O38	1.968(11)
Mn5–O16	2.151(13)	Mn13–O39	2.218(10)
Mn5–O13	2.267(11)	Mn14–O41	1.883(10)
Mn6–O22	1.821(10)	Mn14–O48	1.914(10)
Mn6–O11	1.904(11)	Mn14–O46	1.920(10)
Mn6–O12	1.949(10)	Mn14–O47	2.247(10)
Mn6–O16	2.534(11)	Mn15–O39	1.881(11)
Mn7–O33	1.856(9)	Mn15–O48	1.900(9)
Mn7–O20	1.886(9)	Mn15–O40	1.938(11)
Mn8–O21	1.884(10)	Mn15–O47	2.255(10)
Mn8–O20	1.920(9)	Mn16–O48	1.827(9)
Mn8–O34	1.914(11)		

[a]Corresponding to the bonds shown in Figure 2 (top). [b]See Table S1 in the Supporting Information for a full listing of distances and angles in the core.

The core of **3** is similar to those of previous Mn_{16} clusters reported by King et al.[26] and Price et al.,[42] which were obtained via reductive aggregation or comproportionation, respectively. Other than MeOH vs H_2O changes, the main difference between **3** and the others occurs in the ligation, the four η^1:η^1:μ-bridging NO_3^- groups replacing four carboxylates. This is still a very rare occurrence in Mn[39,43,44] or mixed Mn/Ln (Ln = lanthanide)[45−47] cluster chemistry, with only a few examples of each. In the present case, as in previous ones, where comparisons are possible, the substitution does not cause significant changes to the core metric parameters. In fact, the only significant change is the Mn–O(nitrate) bonds (average of ~2.27 Å, all on Mn^{III} JT elongation axes) being slightly longer

DOI: 10.1021/acs.inorgchem.5b01553
Inorg. Chem. 2015, 54, 9127−9137

Table 3. Bond Valence Sums and Assignments for Mn and O Atoms in 2 and 3

atom[a]	Mn^{II}	Mn^{III}	Mn^{IV}	atom[b]	BVS	assignment
			Complex 2			
Mn1	2.98	2.72	2.86	O1	1.06	OH^-
Mn2	3.31	3.03	3.17	O10	1.95	MeO^-
Mn3	3.07	2.81	2.95	O11	2.08	MeO^-
Mn4	3.19	2.92	3.06	O13	1.91	MeO^-
Mn5	3.27	2.99	3.15	O14	1.99	MeO^-
Mn6	3.22	2.95	3.10	O15	1.16	OH^-
Mn7	3.31	3.03	3.18	O17	1.12	MeOH
Mn8	3.23	2.95	3.10	O27	1.18	MeOH
Mn9	3.06	2.79	2.94	O37	0.78	MeOH
Mn10	3.27	2.99	3.14	O38	1.09	OH^-
Mn11	3.23	2.95	3.10	O39	1.99	MeO^-
Mn12	3.18	2.91	3.05	O40	2.01	MeO^-
Mn13	3.17	2.90	3.05	O46	2.10	MeO^-
Mn14	3.36	3.07	3.22	O47	1.96	MeO^-
Mn15	3.35	3.06	3.22	O57	1.22	MeOH
Mn16	3.20	2.92	3.07	O59	0.99	MeOH
			Complex 3			
Mn1	4.21	3.85	4.04	O6	2.03	MeO^-
Mn2	4.12	3.77	3.96	O10	2.01	MeO^-
Mn3	3.00	3.01	3.17	O20	1.18	MeOH
Mn4	3.30	3.03	3.18	O25	2.06	MeO^-
Mn5	4.44	4.06	4.26	O29	0.32	H_2O
Mn6	3.33	3.05	3.21	O30	0.26	H_2O
Mn7	3.30	3.03	3.17			
Mn8	3.32	3.03	3.19			

[a]The underlined value is the closest to the charge for which it was calculated. The oxidation state is the nearest whole number to the underlined value. [b]O BVS values in the ranges of ~1.8−2.0, ~1.0−1.2, and ~0.2−0.4 indicate non-, single-, and double-protonation, respectively.

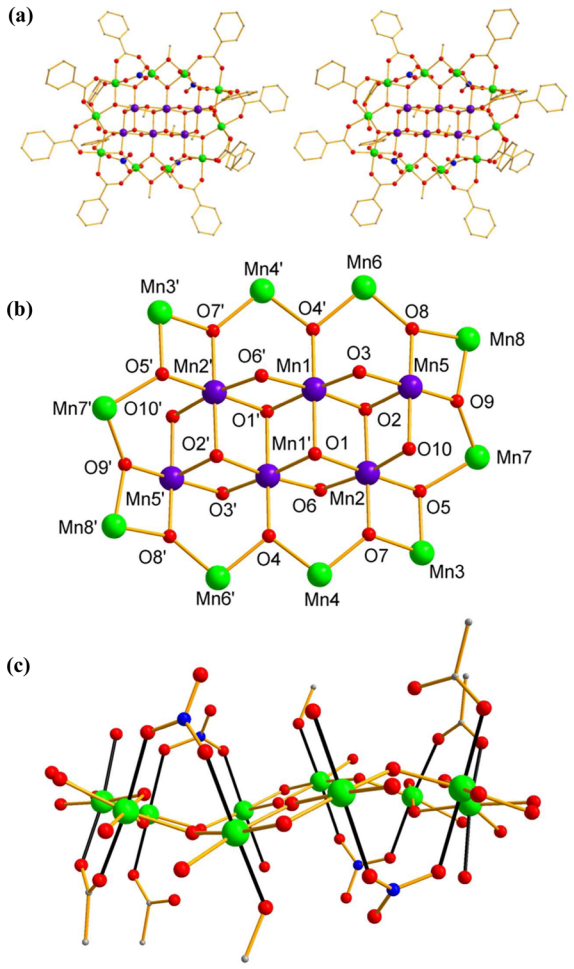

Figure 3. (a) Schematic of a stereopair of the complete structure of complex **3**, (b) the labeled core (the MeO^- O atoms are O6, O6′, O10, and O10′), and (c) the location of the Mn^{III} JT elongation axes (thicker black bonds); for the sake of clarity, only the Mn^{III} atoms are shown. Primed and unprimed atoms are related by the inversion center. Color code: Mn^{III}, green; Mn^{IV}, purple; O, red; C, gray. Hydrogen atoms have been omitted for the sake of clarity.

than the Mn−O(carb) bonds (average of ~2.17) at comparable positions. Nevertheless, this difference leads to very large changes in the magnetic properties (vide infra). In addition, all of the previous examples were with acetate or substituted acetate ($XCH_2CO_2^-$, where X = Cl, Br, or Ph) ligands and all were obtained in low yields (<12%). Thus, the present work has provided both a new member of this series with bulkier aromatic and nitrate ligation, and also a more satisfactory yield of 35% for this interesting cluster type.

Another interesting structural point is that the core of **3** is the central member of a family of structurally related $[Mn^{IV}_mMn^{III}_n]$ clusters with O^{2-}/MeO^-bridges (Figure 4) that currently contains three members of nuclearity $(m + n)$ of Mn_{12},[23] Mn_{16}, and Mn_{21}.[48] They all have a planar $m = x \times y$ central grid, currently spanning 2 × 2, 2 × 3, and 3 × 3, contained within a Mn^{III}_n $(n = 2(x + y) = 8, 10, 12)$ loop. Thus, we can predict the hypothetical next member of this family would be a Mn_{26} cluster, i.e., $[Mn^{IV}_{12}Mn^{III}_{14}]$ from $m = 3 \times 4$ and $n = 2(3 + 4) = 14$.

Magnetochemistry. *DC Magnetic Susceptibility Studies.* Solid-state, variable-temperature magnetic susceptibility (χ_M) data were collected on dried microcrystalline samples in the 5.0−300 K range in a 0.1 T (1000 G) dc magnetic field. The data for **2**·MeOH and **3**·2$MeNO_2$ are plotted as χ_MT vs T in Figure 5.

For **2**·MeOH, χ_MT slowly decreases from 45.59 cm^3 K mol^{-1} at 300 K to 40.69 cm^3 K mol^{-1} at 150 K before steeply increasing to 73.89 cm^3 K mol^{-1} at 14 K and then dropping slightly to 71.00 cm^3 K mol^{-1} at 5.0 K. The 300 K value is slightly less than the spin-only (g = 2.0) value of 48.00 cm^3 K mol^{-1} for 16 noninteracting Mn^{III}atoms, and the overall profile indicates both ferromagnetic (F) and antiferromagnetic (AF) exchange interactions to be present. For **3**·2$MeNO_2$, χ_MT steadily decreases with decreasing temperature from 45.92 cm^3 K mol^{-1} at 300 K to 30.26 cm^3 K mol^{-1} at 5.0 K. The χ_MT at 300 K is greater than the spin-only (g = 2.0) value of 41.25 cm^3 K mol^{-1} expected for 10 Mn^{III} and 6 Mn^{IV}noninteracting ions, which together with the overall profile again indicates the presence of both F and AF interactions. The χ_MT at 5.0 K suggests $S \approx 12$ and $S \approx 7-8$ ground states.

To better determine the ground states and the magnitudes of the zfs parameter D, magnetization (M) data were collected in the magnetization range of 0.1−7 T and the temperature range of 1.8−10 K; these data are plotted as $M/N\mu_B$ vs H/T in Figure 6, where N is Avogadro's number, H is the applied field, and μ_B is the Bohr magneton. The data were fit using the MAGNET program,[38] by diagonalization of the spin Hamiltonian matrix, incorporating axial anisotropy ($D\hat{S}_z^2$) and Zeeman terms, and employing a full powder average.[49] The spin Hamiltonian is given by eq 3,

DOI: 10.1021/acs.inorgchem.5b01553
Inorg. Chem. 2015, 54, 9127−9137

Table 4. Selected Core Interatomic Distances for Complex 3[a]

atom pairing	interatomic distance (Å)	atom pairing	interatomic distance (Å)
Mn1···Mn1′	2.903(2)	Mn2···Mn7	3.452(2)
Mn1···Mn2	2.896(2)	Mn3···Mn4	3.336(2)
Mn1···Mn2′	2.864(2)	Mn3···Mn7	3.316(2)
Mn1···Mn5	2.763(2)	Mn4···Mn6′	2.925(2)
Mn1···Mn4′	3.446(2)	Mn5···Mn6	3.374(2)
Mn1···Mn6	3.417(2)	Mn5···Mn7	3.441(2)
Mn2···Mn3	2.801(2)	Mn5···Mn8	2.792(2)
Mn2···Mn4′	3.399(2)	Mn6···Mn8	3.381(2)
Mn2···Mn5	2.845(2)	Mn7···Mn8	3.406(2)
Mn1−O3	1.842(5)	Mn5−O3	1.841(4)
Mn1−O2	1.896(4)	Mn5−O8	1.862(4)
Mn1−O6	1.906(5)	Mn5−O2	1.891(4)
Mn1−O4	1.910(5)	Mn5−O21	1.900(5)
Mn1−O1	1.929(4)	Mn5−O9	1.908(4)
Mn1−O1′	1.932(4)	Mn5−O10	1.911(4)
Mn2−O7	1.865(5)	Mn6−O8	1.867(4)
Mn2−O5	1.886(4)	Mn6−O4	1.897(4)
Mn2−O1	1.905(4)	Mn6−O25	1.908(5)
Mn2−O2	1.917(4)	Mn6−O23	1.959(5)
Mn2−O6′	1.920(5)	Mn6−O29′	2.150(13)
Mn2−O10	1.925(5)	Mn6−O26	2.227(7)
Mn3−O5	1.884(4)	Mn7−O9	1.859(5)
Mn3−O7	1.904(4)	Mn7−O19	1.941(6)
Mn3−O14	1.945(5)	Mn7−O5	1.948(4)
Mn3−O18	1.950(5)	Mn7−O31	1.967(5)
Mn3−O16	2.112(5)	Mn7−O17	2.070(5)
Mn3−O11	2.286(5)	Mn7−O30	2.232(5)
Mn4−O4′	1.888(5)	Mn8−O9	1.871(4)
Mn4−O7	1.889(4)	Mn8−O8	1.886(4)
Mn4−O25′	1.926(4)	Mn8−O32	1.932(5)
Mn4−O15	1.938(5)	Mn8−O24	1.935(5)
Mn4−O20	2.173(6)	Mn8−O22	2.187(5)
Mn4−O12	2.276(6)	Mn8−O27	2.301(5)

[a]See Table S2 for a fuller listing of distances and angles in the core.

$$\mathcal{H} = D\hat{S}_z^{\,2} + g\mu_B\mu_0\hat{S}\cdot H \qquad (3)$$

where μ_0 is the permeability of a vacuum.

Since **2**·MeOH and **3**·2MeNO$_2$are both high nuclearity, we expected that low-lying excited states might cause problems to the fit, since the model assumes that only the ground state is populated. Indeed, in both cases, we could get no acceptable fits using all data collected. Therefore, we used only data at lower fields (0.1−4.0 T) and temperatures (1.8−4.0 K), which is a common strategy to minimize problems from low-lying excited states; we avoided fields even lower than 0.1 T, to preclude introducing additional problems from weak intermolecular interactions, particularly for **2**·MeOH, which contains a hydrogen-bonded chain structure (vide supra). For **2**·MeOH, a good fit was now obtained with S = 12, D = −0.16(1) cm^{-1}, and g = 1.98(3) (Figure 6a). Similarly, a good fit was now obtained for **3**·2MeNO$_2$ with S = 8, D = −0.22(1) cm^{-1}, and g = 1.99(2) (Figure 6b). The root-mean-square D vs g error surface for the fits for **2**·MeOH and **3**·2MeNO$_2$ were calculated using the GRID program[50] (see Figures S2 and S3, respectively, in the Supporting Information),[41] and they show that the fits are much softer, with respect to g than D, leading to the given estimates of the uncertainties in these parameters. For both fits, there was a local fit minimum with positive D, but these were of much lower quality than the global minima with negative D given above and were discarded; negative D values are expected for JT axially elongated Mn^{III}.[51]

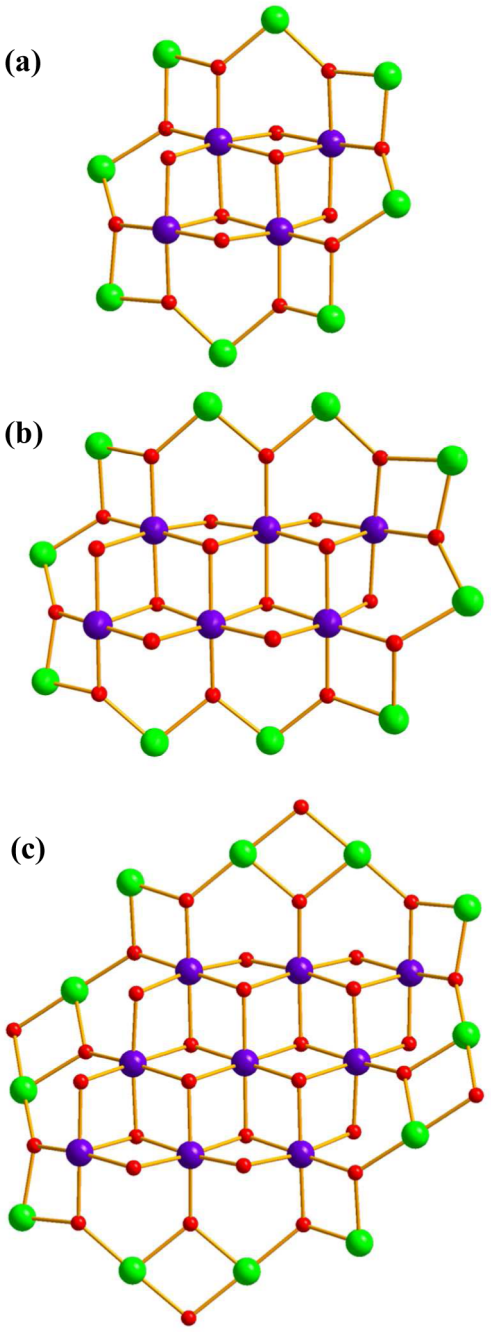

Figure 4. Cores of the (a) Mn_{12}, (b) Mn_{16}, and (c) Mn_{21} members of the $[Mn_m^{IV}Mn_n^{III}]$ family of clusters with a planar $[Mn_m^{IV}]$ grid held within a nonplanar $[Mn_n^{III}]$ loop. The Mn^{IV} atoms are bridged by a mix of O^{2-} and MeO^- ions. Color code: Mn^{IV}, purple; Mn^{III}, green; O, red.

AC Magnetic Susceptibility Studies. In order to further probe the ground states of **2**·MeOH and **3**·2MeNO$_2$, and to determine the magnetization dynamics, ac susceptibility data were collected in the temperature range of 1.8−15 K in a 3.5 G ac field at frequencies in the 0.1−1500 Hz range. The in-phase ac susceptibility (χ'_M) for **2**·MeOH, shown as χ'_MT vs T in Figure 7a, is essentially constant at ∼78 cm^3 K mol^{-1} in the 9.0−15 K range, indicating an S = 12 ground state (spin-only (g

DOI: 10.1021/acs.inorgchem.5b01553
Inorg. Chem. 2015, 54, 9127−9137

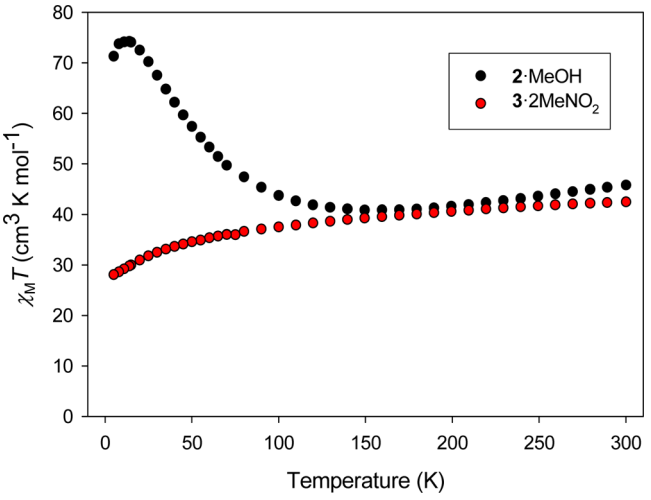

Figure 5. $\chi_M T$ vs T plots for **2**·MeOH and **3**·2MeNO$_2$ in a 1000 G dc field.

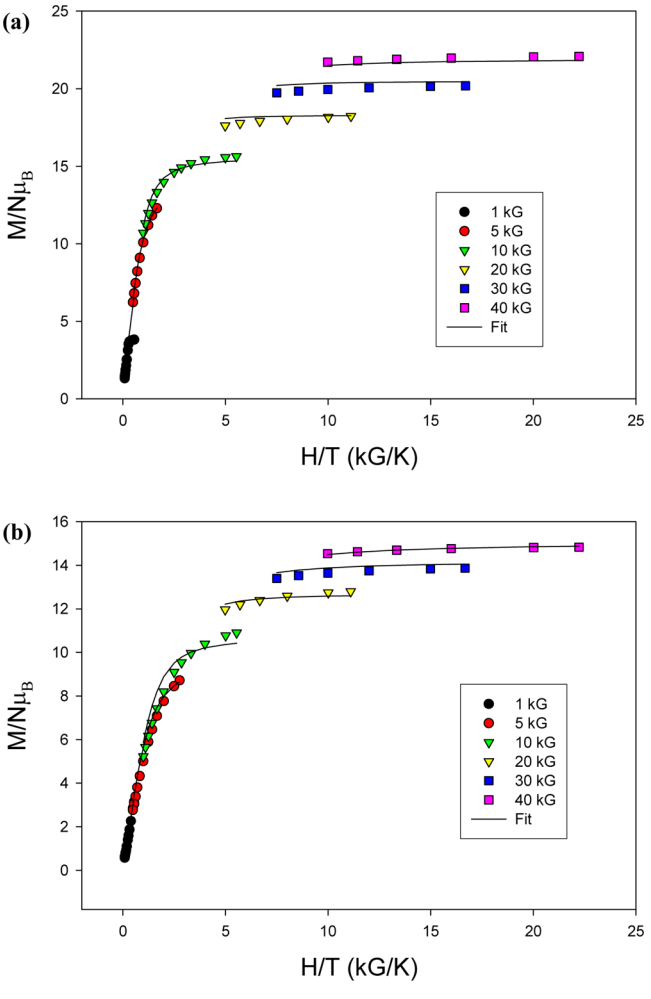

Figure 6. Reduced magnetization ($M/N\mu_\beta$) vs H/T plots for (a) **2**·MeOH and (b) **3**·2MeNO$_2$ at the indicated dc fields. The solids line are the fit of the data; see text for the fit parameters.

= 2) value for S = 12 is 78.00 cm^3 K mol^{-1}) in agreement with the dc data. Below 9.0 K, there is a frequency-dependent decrease in $\chi'_M T$ concomitant with appearance of frequency-dependent out-of-phase ac susceptibility (χ''_M) signals (Figure

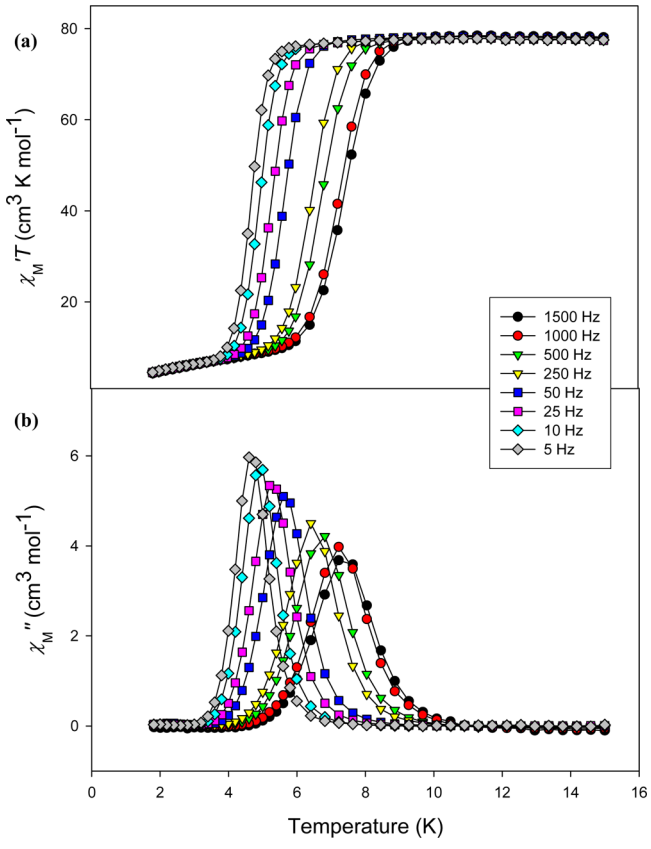

Figure 7. (a) $\chi'_M T$ vs T and (b) χ''_M vs T ac susceptibility plots for **2**·MeOH at the indicated frequencies. The solid lines are present to serve as guides for the eye.

7b), characteristic of the slow magnetization relaxation of a SMM.

The χ''_M vs T plots were used as a source of kinetic data to calculate the effective energy barrier (U_{eff}) to magnetization relaxation.[2,52] The χ''_M peak temperature (T_{max}) at each of 25 frequencies in the 5−1500 Hz range was used to obtain relaxation rate ($1/\tau$) vs T data,[2] where τ is the relaxation time, which was used to construct an Arrhenius plot of $\ln(1/\tau)$ vs $1/T$ (Figure 8) based on eq 4:

$$\left(\frac{1}{\tau}\right) = \left(\frac{1}{\tau_0}\right)\exp\left(-\frac{U_{eff}}{kT}\right) \quad (4)$$

A linear fit gave U_{eff} = 49.7(1) K and $\tau_0 = 4.32 \times 10^{-9}$ s. We could detect no significant curvature in the data and, therefore, did not attempt a fit to the double exponential version of eq 4.[53] The U_{eff} for **2**·MeOH is one of the largest for homometallic Mn$_x$ SMMs, being only slightly smaller, for example, than those for the [Mn$_{12}$O$_{12}$(O$_2$CR)$_{16}$(H$_2$O)$_4$] family (typical U_{eff} = 60−65 K).

AC in-phase and out-of-phase susceptibility vs frequency data (Figure S4 in the Supporting Information) were collected at T = 6.0 K to allow an Argand (Cole−Cole) plot to be constructed.[2] The resulting χ'_M vs χ''_M plot for frequencies in the 0.1−1500 Hz range is shown in Figure 9. The data were subjected to a least-squares fit to a single relaxation process (dashed line in Figure 9) and a distribution of single relaxation processes (solid line in Figure 9), based on the corresponding equations given elsewhere.[2] A distribution of single relaxation processes corresponds to a small range of U_{eff} barrier values, as

DOI: 10.1021/acs.inorgchem.5b01553
Inorg. Chem. 2015, 54, 9127−9137

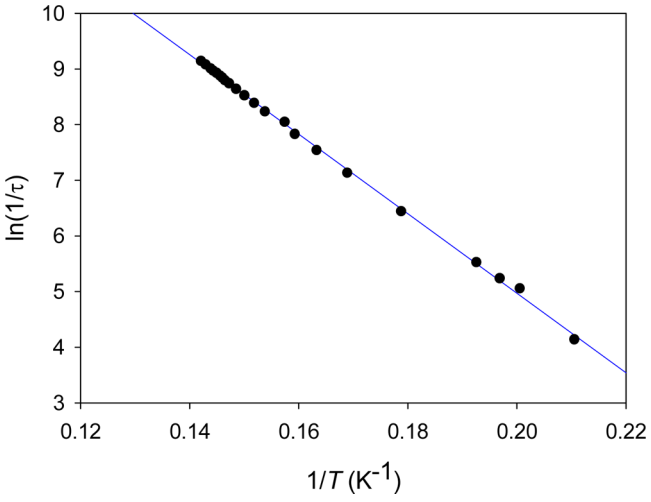

Figure 8. Arrhenius $\ln(1/\tau)$ vs $1/T$plot for **2**·MeOH. The fit to eq 4 is shown as a solid line; see text for the fit parameters.

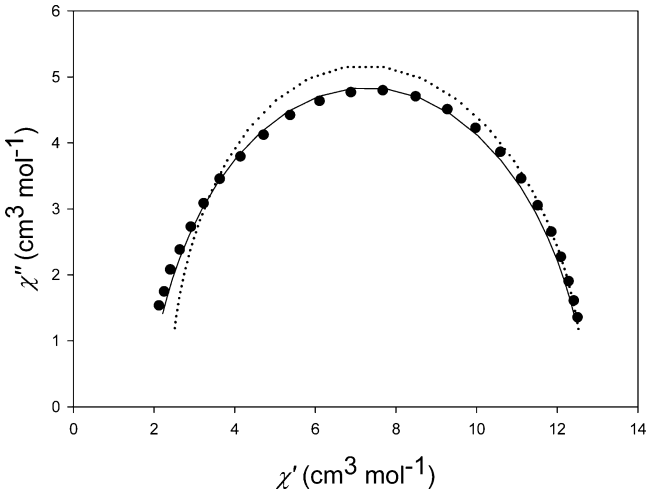

Figure 9. χ'_M vs χ''_M Argand plot for **2**·MeOH at T = 6.00 K. The dashed line is the fit of the data to a single relaxation process, and the solid line is a fit to a distribution of single relaxation processes. See text for details and the fit parameters.

would be expected from the distribution of molecular environments in a typical molecular crystal, with parameter α gauging the width of the distribution. The fit of the data to a distribution with α = 0.071 (solid line) is clearly superior to the fit to a single relaxation process. The relaxation times from the two fits were similar: τ = 0.0014 and 0.0015 s, respectively. The small value of α indicates a small distribution of molecular environments, as expected for a molecular crystal displaying minor types of ligand, solvent, and other disorders; in fact, this is smaller than those for many other Mn_x SMMs.[54]

For **3**·2MeNO$_2$, $\chi'_M T$ decreases from ~34 cm^3 K mol^{-1} at 15 K to a minimum of ~32 cm^3 K mol^{-1} at 5.0 K before increasing to a maximum (at 50 Hz) of ~35 cm^3 K mol^{-1} at 2.0 K (Figure 10a). The latter is consistent with an S = 8 ground state (spin-only value 36 cm^3 K mol^{-1}) and g < 2 slightly, as expected for Mn^{III}, in excellent agreement with the conclusion from the dc magnetization fit. The decreasing $\chi'_M T$ below 15 K indicates depopulation of low-lying excited states, and the increase below 5.0 K is assigned to depopulation of an excited state (or states) with S < 8 that are very low-lying. The presence of low-lying

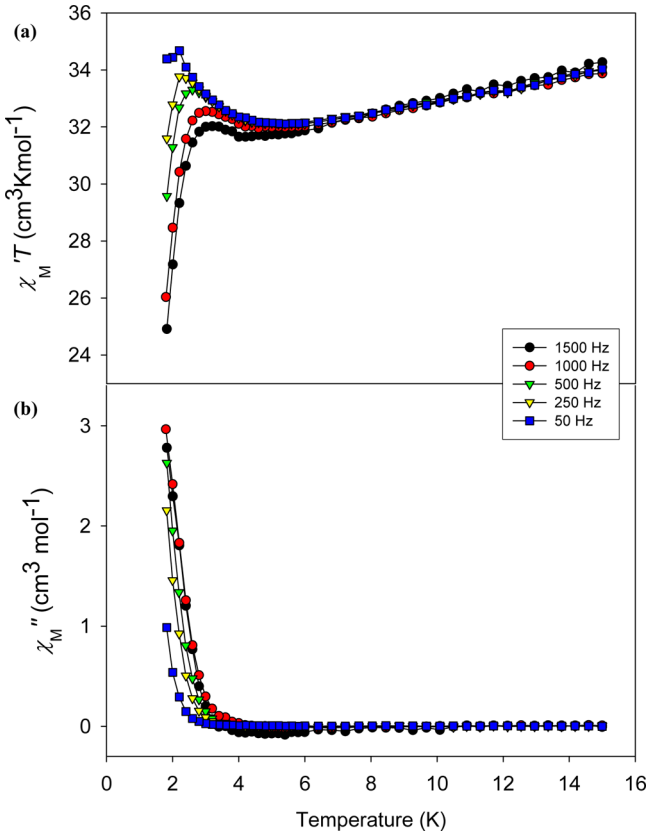

Figure 10. (a) $\chi'_M T$ vs T and (b) χ''_M vs T ac susceptibility plots for **3**·2MeNO$_2$ at the indicated frequencies. The solid lines are present to serve as guides for the eye.

excited states rationalizes the problems encountered in the magnetization fits. Below 2.0 K at 50 Hz, and at higher temperatures at higher frequencies, there is a frequency-dependent decrease and concomitant appearance of frequency-dependent out-of-phase χ''_M signals characteristic of a SMM (Figure 10b). However, the χ''_M signals are merely the tails of peaks lying at <1.8 K, which was the limit of our instrument.

The S = 8 ground state is markedly different from the S = 2 ground state[26] and the S = 3 or 4 ground state[42] found in previous Mn_{16} complexes with the same core; we assign this difference primarily to the bridging nitrates. The longer Mn−O bonds on the local Mn^{III} z-axes will affect the energy of eight d_{z^2} magnetic orbitals, affecting the exchange couplings (J_{ij}) with neighboring Mn atoms. The changes in J_{ij} are unlikely to be large; however, in such high-nuclearity systems involving many spin-frustrated triangular Mn_3 subunits from competing interactions, the ground state is often very sensitive to even small changes in the relative magnitude of the competing interactions.[55,56]

In order to obtain an estimate of U_{eff} and τ_0 for **3**·2MeNO$_2$ in the absence of χ''_M peak T vs frequency data, we instead used the χ'_M and χ''_M for the tails at four frequencies (υ) and at different T to construct a $\log(\chi''_M/\chi'_M)$ vs $1/T$ plot (Figure 11), based on the Kramers−Kronig equation (eq 5),[57]

$$\log\left(\frac{\chi''_M}{\chi'_M}\right) = \log(\omega\tau_0) + \frac{U_{eff}}{k_B T} \quad (5)$$

where ω is the angular frequency of the ac field ($\omega = 2\pi\upsilon$). Fitting the data and averaging the obtained parameters gave U_{eff}

DOI: 10.1021/acs.inorgchem.5b01553
Inorg. Chem. 2015, 54, 9127−9137

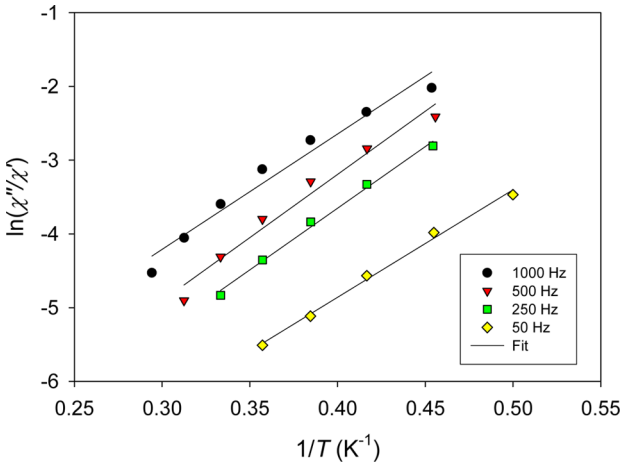

Figure 11. Plot of $\ln(\chi''/\chi')$ vs 1/T for **3**·2MeNO$_2$ in zero-applied field at the indicated ac frequencies. The solid lines are fits of the data; see text for the fit parameters.

$\approx 14 \pm 2$ cm^{-1} and $\tau_0 \approx (3.2 \pm 0.5) \times 10^{-8}$ s. This is a reasonable approximation for U_{eff}, because the upper limit to the barrier ($U = S^2|D|$) is estimated at $U = 14$ cm^{-1}, using the values $S = 8$ and $D = -0.22$ cm^{-1} from the fit of dc magnetization data.

CONCLUSIONS

Two new clusters are reported that are the latest members of a growing family of Mn_{16} molecules[26,42,58−67] that already spans a wide range of structural types and interesting physical properties, including single-molecule magnetism. These new members are, nevertheless, extremely interesting in their own individual and distinct ways. One of them, complex **2**, is an unprecedented structural type, consisting of an unusual W-shaped pleated topology of Mn^{III} atoms and quite a high barrier to magnetization relaxation, which is almost comparable to the $[Mn_{12}O_{12}(O_2CR)_{16}(H_2O)_4]$ family of prototypical SMMs. The results described also continue to support the utility of the reductive aggregation methodology as a route to high-nuclearity clusters with remarkable structural and magnetic properties. Complex **3** was obtained from a new synthetic procedure and is another recent example showing that, although nitrate groups are not normally considered excellent bridging ligands, they will occasionally be found in carboxylate-like bridging modes in Mn cluster chemistry. More importantly, this will often lead to markedly altered magnetic properties, compared with the analogous carboxylate-bridged cluster, if it is available for comparative study. In the present case, a higher ground state (S) results for **3** than for previous Mn_{16} clusters with the same core. If a straightforward nitrate-for-carboxylate substitution procedure could be developed, this might even prove to be a controlled way to alter the ground state and/or increase the magnitude of the zfs parameter (D) of a Mn SMM, as a result of the longer JT axial bonds. The one reported procedure involving treatment with nitric acid requires great care.[43] The synthetic procedures described in this work continue to be explored in various ways in our group, and additional results will be reported in due course.

ASSOCIATED CONTENT

Supporting Information

The Supporting Information is available free of charge on the ACS Publications website at DOI: 10.1021/acs.inorgchem.5b01553.

Structural figure for **2**·MeOH, extended tables of selected bond distances and angles, and error surface plots for D vs g fits (PDF)

Crystallographic information for **2**·MeOH and **3**·2MeNO$_2$ (CIF)

AUTHOR INFORMATION

Corresponding Author

*Tel.: +1-352-392-8314. Fax: +1-352-392-8757. E-mail: christou@chem.ufl.edu.

Notes

The authors declare no competing financial interest.

ACKNOWLEDGMENTS

We thank the National Science Foundation (Grant No. DMR-1213030) for support of this work.

REFERENCES

(1) (a) Christou, G.; Gatteschi, D.; Hendrickson, D. N.; Sessoli, R. *MRS Bull.* **2000**, *25*, 66−71. (b) Gatteschi, D.; Sessoli, R. *Angew. Chem., Int. Ed.* **2003**, *42*, 268−297. (c) Christou, G. *Polyhedron* **2005**, *24*, 2065−2075. (d) Aromi, G.; Brechin, E. K. *Struct. Bonding (Berlin)* **2006**, *122*, 1−67.

(2) Bagai, R.; Christou, G. *Chem. Soc. Rev.* **2009**, *38*, 1011−1026.

(3) Woodruff, D. N.; Winpenny, R. E.; Layfield, R. A. *Chem. Rev.* **2013**, *113*, 5110−5148.

(4) Rinehart, J. D.; Long, J. R. *J. Am. Chem. Soc.* **2009**, *131*, 12558−12559.

(5) (a) Pereira, L. C. J.; Camp, C.; Coutinho, J. T.; Chatelain, L.; Maldivi, P.; Almeida, M.; Mazzanti, M. *Inorg. Chem.* **2014**, *53*, 11809−11811. (b) Moro, F.; Mills, D. P.; Liddle, S. T.; van Slageren, J. *Angew. Chem., Int. Ed.* **2013**, *52*, 3430−3433.

(6) Craig, G. A.; Murrie, M. *Chem. Soc. Rev.* **2015**, *44*, 2135−2147.

(7) (a) Rinehart, J. D.; Fang, M.; Evans, W. J.; Long, J. R. *Nat. Chem.* **2011**, *3*, 538−542. (b) Rinehart, J. D.; Fang, M.; Evans, W. J.; Long, J. R. *J. Am. Chem. Soc.* **2011**, *133*, 14236−14239.

(8) (a) Friedman, J. R.; Sarachik, M. P.; Tejada, J.; Ziolo, R. *Phys. Rev. Lett.* **1996**, *76*, 3830−3833. (b) Thomas, L.; Lionti, F.; Ballou, R.; Gatteschi, D.; Sessoli, R.; Barbara, B. *Nature* **1996**, *383*, 145−147.

(9) Wernsdorfer, W.; Aliaga-Alcalde, N.; Hendrickson, D. N.; Christou, G. *Nature* **2002**, *416*, 406−409.

(10) (a) Hill, S.; Edwards, R. S.; Aliaga-Alcalde, N.; Christou, G. *Science* **2003**, *302*, 1015−1018. (b) Tiron, R.; Wernsdorfer, W.; Foguet-Albiol, D.; Aliaga-Alcalde, N.; Christou, G. *Phys. Rev. Lett.* **2003**, *91*, 227203.

(11) (a) Wernsdorfer, W.; Sessoli, R. *Science* **1999**, *284*, 133−135. (b) Wernsdorfer, W.; Soler, M.; Christou, G.; Hendrickson, D. N. *J. Appl. Phys.* **2002**, *91*, 7164−7166. (c) Wernsdorfer, W.; Chakov, N. E.; Christou, G. *Phys. Rev. Lett.* **2005**, *95*, 037203.

(12) Bircher, R.; Chaboussant, G.; Dobe, C.; Gudel, H. U.; Ochsenbein, S. T.; Sieber, A.; Waldmann, O. *Adv. Funct. Mater.* **2006**, *16*, 209−220.

(13) (a) Brechin, E. *Chem. Commun.* **2005**, *41*, 5141−5153. (b) Tasiopoulos, A. J.; Perlepes, S. P. *Dalton Trans.* **2008**, *41*, 5537−5555. (c) Kostakis, G. E.; Ako, A. M.; Powell, A. K. *Chem. Soc. Rev.* **2010**, *39*, 2238−2271. (d) Arom, G.; Aubin, S. M. J.; Bolcar, M. A.; Christou, G.; Eppley, H. J.; Folting, K.; Hendrickson, D. N.; Huffman, J. C.; Squire, R. C.; Tsai, H. L.; Wang, S.; Wemple, M. W. *Polyhedron* **1998**, *17*, 3005−3020.

DOI: 10.1021/acs.inorgchem.5b01553
Inorg. Chem. 2015, 54, 9127−9137

(14) (a) Moushi, E. E.; Stamatatos, T. C.; Wernsdorfer, W.; Nastopoulos, V.; Christou, G.; Tasiopoulos, A. J. *Inorg. Chem.* **2009**, *48*, 5049−5051.
(15) Ako, A. M.; Hewitt, I. J.; Mereacre, V.; Clerac, R.; Wernsdorfer, W.; Anson, C. E.; Powell, A. K. *Angew. Chem., Int. Ed.* **2006**, *45*, 4926−4929.
(16) Stamatatos, T. C.; Abboud, K. A.; Wernsdorfer, W.; Christou, G. *Angew. Chem., Int. Ed.* **2007**, *46*, 884−888.
(17) Waldmann, O. *Inorg. Chem.* **2007**, *46*, 10035−10037.
(18) Lis, T. *Acta Crystallogr., Sect. B: Struct. Crystallogr. Cryst. Chem.* **1980**, *B36*, 2042−2046.
(19) Tasiopoulos, A. J.; Vinslava, A.; Wernsdorfer, W.; Abboud, K. A.; Christou, G. *Angew. Chem., Int. Ed.* **2004**, *43*, 2117−2121.
(20) (a) Whitehead, G. F. S.; Ferrando-Soria, J.; Christie, L. G.; Chilton, N. F.; Timco, G. A.; Moro, F.; Winpenny, R. E. P. *Chem. Sci.* **2014**, *5*, 235−239. (b) Whitehead, G. F. S.; Moro, F.; Timco, G. A.; Wernsdorfer, W.; Teat, S. J.; Winpenny, R. E. P. *Angew. Chem., Int. Ed.* **2013**, *52*, 9932−9935. (c) Ferrando-Soria, J.; Fernandez, A.; Moreno Pineda, E.; Varey, S. A.; Adams, R. W.; Vitorica-Yrezabal, I. J.; Tuna, F.; Timco, G. A.; Muryn, C. A.; Winpenny, R. E. P. *J. Am. Chem. Soc.* **2015**, *137*, 7644−7647.
(21) (a) Mowson, A. M.; Nguyen, T. N.; Abboud, K. A.; Christou, G. *Inorg. Chem.* **2013**, *52*, 12320−12322. (b) Costa, J. S.; Barrios, L. A.; Craig, G. A.; Teat, S. J.; Luis, F.; Roubeau, O.; Evangelisti, M.; Camon, A.; Aromi, G. *Chem. Commun.* **2012**, *48*, 1413−1415. (c) Aromı, G.; Aguila, D.; Gamez, P.; Luis, F.; Roubeau, O. *Chem. Soc. Rev.* **2012**, *41*, 537−546.
(22) Mukherjee, S.; Abboud, K. A.; Wernsdorfer, W.; Christou, G. *Inorg. Chem.* **2013**, *52*, 873−884.
(23) Tasiopoulos, A. J.; Wernsdorfer, W.; Abboud, K. A.; Christou, G. *Angew. Chem., Int. Ed.* **2004**, *43*, 6338−6342.
(24) Tasiopoulos, A. J.; Wernsdorfer, W.; Abboud, K. A.; Christou, G. *Inorg. Chem.* **2005**, *44*, 6324−6338. Tasiopoulos, A. J.; Wernsdorfer, W.; Abboud, K. A.; Christou, G. *Polyhedron* **2005**, *24*, 2505−2512.
(25) King, P.; Wernsdorfer, W.; Abboud, K. A.; Christou, G. *Inorg. Chem.* **2005**, *44*, 8659−8669.
(26) King, P.; Wernsdorfer, W.; Abboud, K. A.; Christou, G. *Inorg. Chem.* **2004**, *43*, 7315−7323.
(27) Tasiopoulos, A. J.; Wernsdorfer, W.; Moulton, B.; Zaworotko, M. J.; Christou, G. *J. Am. Chem. Soc.* **2003**, *125*, 15274−15275.
(28) (a) Tasiopoulos, A. J.; O'Brien, T. A.; Abboud, K. A.; Christou, G. *Angew. Chem., Int. Ed.* **2004**, *43*, 345−349. (b) Tasiopoulos, A. J.; Milligan, P. L., Jr.; Abboud, K. A.; O'Brien, T. A.; Christou, G. *Inorg. Chem.* **2007**, *46*, 9678−9691. (c) Milios, C. J.; Wood, P. A.; Parsons, S.; Foguet-Albiol, D.; Lampropoulos, C.; Christou, G.; Perlepes, S. P.; Brechin, E. K. *Inorg. Chim. Acta* **2007**, *360*, 3932−3940. (d) Mishra, A.; Tasiopoulos, A. J.; Wernsdorfer, W.; Abboud, K. A.; Christou, G. *Inorg. Chem.* **2007**, *46*, 3105−3115.
(29) (a) Mishra, A.; Tasiopoulos, A. J.; Wernsdorfer, W.; Moushi, E. E.; Moulton, B.; Zaworotko, M. J.; Abboud, K. A.; Christou, G. *Inorg. Chem.* **2008**, *47*, 4832−4834. (b) Wang, H. S.; Ma, C. B.; Wang, M.; Chen, C. N.; Liu, Q. T. *J. Mol. Struct.* **2008**, *875*, 288−294. (c) Mereacre, V.; Ako, A. M.; Akhtar, M. N.; Lindemann, A.; Anson, C. E.; Powell, A. K. *Helv. Chim. Acta* **2009**, *92*, 2507−2524. (d) Romanenko, G. V.; Fursova, E. Y.; Ovcharenko, V. I. *Russ. Chem. Bull.* **2009**, *58*, 1−10.
(30) (a) Li, Y. W.; Li, T. G.; Wang, Y. H.; Feng, X. J.; Lu, Y.; Wang, E. B. *Inorg. Chem.* **2009**, *48*, 6452−6458. (b) Akhtar, M. N.; Lan, Y.; Mereacre, V.; Clerac, R.; Anson, C. E.; Powell, A. K. *Polyhedron* **2009**, *28*, 1698−1703. (c) Wang, M.; Yuan, D. Q.; Ma, C. B.; Yuan, M. J.; Hu, M. Q.; Li, N.; Chen, J.; Chen, C. N.; Liu, Q. T. *Dalton Trans.* **2010**, *39*, 7276−7285. (d) Ma, C.-B.; Hu, M.-Q.; Chen, H.; Chen, C.-N.; Liu, Q.-T. *Eur. J. Inorg. Chem.* **2011**, *2011*, 5043−5053.
(31) (a) Wang, H. S.; Pan, Z. Q. *Chin. J. Inorg. Chem.* **2013**, *7*, 1459−1464. (b) Papatriantafyllopoulou, C.; Abboud, K. A.; Christou, G. *Polyhedron* **2013**, *52*, 196−206. (c) Lampropoulos, C.; Thuijs, A. E.; Mitchell, K. J.; Abboud, K. A.; Christou, G. *Inorg. Chem.* **2014**, *53*, 6805−6816. (d) Thuijs, A. E.; Marton, A.; Stamatatos, T. C.; Abboud, K. A.; Christou, G. *Polyhedron* **2015**, DOI: 10.1016/j.poly.2015.03.017.
(32) Vincent, J. B.; Folting, K.; Huffman, J. C.; Christou, G. *Inorg. Chem.* **1986**, *25* (7), 996−999.
(33) (a) Wang, S.; Huffman, J. C.; Folting, K.; Streib, W. E.; Lobkovsky, E. B.; Christou, G. *Angew. Chem., Int. Ed. Engl.* **1991**, *30*, 1672−1674. (b) Wemple, M. W.; Tsai, H.-L.; Wang, S.; Claude, J.-P.; Streib, W. E.; Huffman, J. C.; Hendrickson, D. N.; Christou, G. *Inorg. Chem.* **1996**, *35*, 6437−6449.
(34) *SHELXTL6*; Bruker−AXS: Madison, WI, 2008.
(35) van der Sluis, P.; Spek, A. L. *Acta Crystallogr., Sect. A: Found. Crystallogr.* **1990**, *A46*, 194−201.
(36) Spek, A. L. *Acta Crystallogr., Sect. D: Biol. Crystallogr.* **2009**, *D65*, 148−155.
(37) Weast, R. C. *CRC Handbook of Chemistry and Physics*; CRC Press: Boca Raton, FL, 1984.
(38) Davidson, E. R. *MAGNET*; Indiana University: Bloomington, IN, 1999.
(39) Thuijs, A. E.; Christou, G.; Abboud, K. A. *Acta Crystallogr., Sect. C: Struct. Chem.* **2015**, *71*, 185−187.
(40) Skoog, D. A.; West, D. M.; Holler, F. J. *Analytical Chemistry: An Introduction*, 5th Edition; Saunders College Publications: Philadelphia, PA, 1990.
(41) See the Supporting Information.
(42) Price, D. J.; Batten, S. R.; Moubaraki, B.; Murray, K. S. *Polyhedron* **2007**, *26*, 305−317.
(43) Artus, P.; Boskovic, C.; Yoo, Y.; Streib, W. E.; Brunel, L.-C.; Hendrickson, D. N.; Christou, G. *Inorg. Chem.* **2001**, *40*, 4199−4210.
(44) Hänninen, M. M.; Välivaara, J.; Mota, A. J.; Colacio, E.; Lloret, F.; Sillanpää, R. *Inorg. Chem.* **2013**, *52*, 2228−2241 10.1021/ic302731z.
(45) Boron, T. T.; Kampf, J. W.; Pecoraro, V. L. *Inorg. Chem.* **2010**, *49*, 9104−9106.
(46) Mereacre, V.; Lan, Y.; Wernsdorfer, W.; Anson, C. E.; Powell, A. K. *C. R. Chim.* **2012**, *15*, 639−646.
(47) Papatriantafyllopoulou, C.; Wernsdorfer, W.; Abboud, K. A.; Christou, G. *Inorg. Chem.* **2011**, *50*, 421−423.
(48) Brockman, J. T.; Huffman, J. C.; Christou, G. *Angew. Chem., Int. Ed.* **2002**, *41*, 2506−2508.
(49) Aliaga-Alcalde, N.; Edwards, R. S.; Hill, S. O.; Wernsdorfer, W.; Folting, K.; Christou, G. *J. Am. Chem. Soc.* **2004**, *126*, 12503−12516.
(50) Davidson, E. R. *GRID*; Indiana University: Bloomington, IN, 1999.
(51) Kennedy, B. J.; Murray, K. S. *Inorg. Chem.* **1985**, *24*, 1552−1557.
(52) Novak, M. A.; Sessoli, R. In *Quantum Tunneling of Magnetization−QTM '94*; Gunther, L., Barbara, B., Eds.; Kluwer: Dordrecht, The Netherlands, 1995; pp 171−188.
(53) Lampropoulos, C.; Murugesu, M.; Harter, A. G.; Wernsdofer, W.; Hill, S.; Dalal, N. S.; Reyes, A. P.; Kuhns, P. L.; Abboud, K. A.; Christou, G. *Inorg. Chem.* **2013**, *52*, 258−272.
(54) (a) Boskovic, C.; Brechin, E.; Streib, W. E.; Folting, K.; Bollinger, J. C.; Hendrickson, D. N.; Christou, G. *J. Am. Chem. Soc.* **2002**, *124*, 3725−3736. (b) Haryono, M.; Kalisz, M.; Sibille, R.; Lescouezec, R.; Fave, C.; Trippe-Allard, G.; Li, Y.; Seuleiman, M.; Rousseliere, H.; Balkhy, A. M.; Lacroix, J. C.; Journaux, J. *Dalton Trans.* **2010**, *39*, 4751−4756. (c) Wu, C.; Datta, S.; Wernsdorfer, W.; Lee, G.; Hill, S.; Yang, E. *Dalton Trans.* **2010**, *39*, 10160−10168.
(55) Stamatatos, T. C.; Foguet-Albiol, D.; Poole, K. M.; Wernsdorfer, W.; Abboud, K. A.; O'Brien, T. A.; Christou, G. *Inorg. Chem.* **2009**, *48*, 9831−9845.
(56) Kahn, O. *Molecular Magnetism*; VCH: Weinheim, Germany, 1993.
(57) (a) Bartolomè, J.; Filoti, G.; Kuncser, V.; Schinteie, G.; Mereacre, V.; Anson, C. E.; Powell, A. K.; Prodius, D.; Turta, C. *Phys. Rev. B: Condens. Matter Mater. Phys.* **2009**, *80*, 014430. (b) Ishikawa, R.; Miyamoto, R.; Nojiri, H.; Breedlove, B. K.; Yamashita, M. *Inorg. Chem.* **2013**, *52*, 8300−8302.
(58) (a) Dawe, L. N.; Shuvaev, K. V.; Thompson, L. K. *Inorg. Chem.* **2009**, *48*, 3323−3341. (b) Dey, S. K.; Thompson, L. K.; Dawe, L. N. *Chem. Commun.* **2006**, *47*, 4967−4969.

DOI: 10.1021/acs.inorgchem.5b01553
Inorg. Chem. 2015, 54, 9127−9137

(59) Liu, W.; Lee, K.; Park, M.; John, R. P.; Moon, D.; Zou, Y.; Liu, X.; Ri, H.-C.; Kim, G. H.; Lah, M. S. *Inorg. Chem.* **2008**, *47*, 8807−8812.
(60) Wang, H.; Zhang, Z.; Song, X.; Zhang, J.; Zhou, H.; Wang, J.; Song, Y.; You, X. *Dalton Trans.* **2011**, *40*, 2703−2706.
(61) Murugesu, M.; Wernsdorfer, W.; Abboud, K. A.; Christou, G. *Angew. Chem., Int. Ed.* **2005**, *44*, 892−896.
(62) Konar, S.; Clearfield, A. *Inorg. Chem.* **2008**, *47*, 3489−3491.
(63) Shah, S. J.; Ramsey, C. M.; Heroux, K. J.; O'Brien, J. R.; DiPasquale, A. G.; Rheingold, A. L.; del Barco, E.; Hendrickson, D. N. *Inorg. Chem.* **2008**, *47*, 6245−6253.
(64) Taguchi, T.; Wernsdorfer, W.; Abboud, K. A.; Christou, G. *Inorg. Chem.* **2010**, *49*, 10579−10589.
(65) (a) Manoli, M.; Prescimone, A.; Mishra, A.; Parsons, S.; Christou, G.; Brechin, E. K. *Dalton Trans.* **2007**, *5*, 532−534. (b) Manoli, M.; Prescimone, A.; Bagai, R.; Mishra, A.; Murugesu, M.; Parsons, S.; Wernsdorfer, W.; Christou, G.; Brechin, E. K. *Inorg. Chem.* **2007**, *46*, 6968−6979.
(66) Alexandropoulos, D. I.; Papatriantafyllopoulou, C.; Li, C.; Cunha-Silva, L.; Manos, M. J.; Tasiopoulos, A. J.; Wernsdorfer, W.; Christou, G.; Stamatatos, T. C. *Eur. J. Inorg. Chem.* **2013**, *2013*, 2286−2290.
(67) Dey, S. K.; Abedin, T. S. M.; Dawe, L. N.; Tandon, S. S.; Collins, J. L.; Thompson, L. K.; Postnikov, A. V.; Alam, M. S.; Müller, P. *Inorg. Chem.* **2007**, *46*, 7767−7781.

DOI: 10.1021/acs.inorgchem.5b01553
Inorg. Chem. 2015, 54, 9127−9137